

Better than Counting: Density Profiles from Force Sampling

Daniel de las Heras¹ and Matthias Schmidt¹

¹*Theoretische Physik II, Physikalisches Institut, Universität Bayreuth, D-95440 Bayreuth, Germany*

(Dated: 30 October 2017, revised version: 31 January 2018)

Calculating one-body density profiles in equilibrium via particle-based simulation methods involves counting of events of particle occurrences at (histogram-resolved) space points. Here we investigate an alternative method based on a histogram of the local force density. Via an exact sum rule the density profile is obtained with a simple spatial integration. The method circumvents the inherent ideal gas fluctuations. We have tested the method in Monte Carlo, Brownian Dynamics and Molecular Dynamics simulations. The results carry a statistical uncertainty smaller than that of the standard, counting, method, reducing therefore the computation time.

The microscopic one-body density distribution $\rho(\mathbf{r})$ is arguably the most important order parameter in simple fluids. While in homogeneous bulk fluid states $\rho = \text{const}$, in crystals the density “profile” is peaked at the lattice sites. There is a multitude of physically interesting situations where the density $\rho \neq \text{const}$, such as for fluids in capillaries, across interfaces, under the action of external fields, etc. Accurate measurements of $\rho(\mathbf{r})$ are very valuable e.g. in order to study wetting properties [1, 2], capillary effects [3], and crystal nucleation [4] on substrates, to characterize the intrinsic liquid-vapor interface [5] and out-of-equilibrium phase coexistence [6], to determine the charge distributions in capacitors [7, 8], and the superadiabatic forces in Brownian systems [9], as well as to obtain information about the bulk phase behaviour in sedimentation-diffusion-equilibrium [10–12]. Furthermore, within density functional theory (DFT) [13, 14], the one-body density attains a fundamental role in the Mermin-Evans extremal principle that determines all thermodynamic and structural properties of the system. High quality simulation data is necessary for the development and assessment of modern DFT approximations [15].

Experimentally, $\rho(\mathbf{r})$ is accessible by a multitude of methods. Examples in colloidal systems are the analysis of confocal microscopy data [16, 17], total internal reflection microscopy near substrates [18], and turbidity measurements [19]. In molecular systems $\rho(\mathbf{r})$ can be measured via three-dimensional AFM scanning [20].

Mathematically, the one-body density distribution is defined as

$$\rho(\mathbf{r}) = \left\langle \sum_i \delta(\mathbf{r} - \mathbf{r}_i) \right\rangle, \quad (1)$$

where \mathbf{r} indicates the spatial argument, the sum runs over all particles, $\delta(\cdot)$ indicates the Dirac distribution, \mathbf{r}_i is the position of particle i and the angles denote the statistical average, which in equilibrium is carried out over the appropriate (e.g. canonical) ensemble.

The standard particle-based approach to sample $\rho(\mathbf{r})$ is to discretize the Dirac function and to count events in a histogram, labelled by position \mathbf{r} and with bins of

a certain size ΔV . Normalization by ΔV and by the number of sampling sweeps ensures the correct normalization, $\int d\mathbf{r} \rho(\mathbf{r}) = N$, where N is the total number of particles. For cases of additional symmetry, such as e.g. planar problems between, say, parallel walls, the density profile might depend only on a reduced number of coordinates, say $\rho(z)$ where z is the coordinate perpendicular to the walls. In practice brute force can be required to obtain accurate data.

We investigate here an alternative method to sample $\rho(\mathbf{r})$, based on a histogram of the local force density. Working on the level of force densities has been suggested before. In particular, Borgis *et al* [21], following the ideas of Assaraf *et al* [22] for quantum systems, describe a variety of advanced methods for sampling the pair distribution function and the one-body density profile in classical systems. The approach described in Ref. [21] is based on expressing formally the delta function in (1) in a mathematically analogous way to the treatment of a point charge in electrostatics. This allows to sample distribution functions that correspond to the electrostatic potential in the analogy. (The systems considered do not need to carry actual charges for their approach to work.) The authors find a reduced variance in the results that they obtain for the distribution functions of interest. Furthermore the force density plays a central role in advanced (adaptive resolution) Molecular Dynamics methods, as exemplified by the work of Fritsch *et al* [23]. The force density is also relevant for investigations of the potential of mean force, although in the current work, we do not specify any particular (reaction) coordinate, as is typically done in characterizing complex systems by a coarse-grained potential of mean force.

We work on the level of the equilibrium force density balance [24]

$$\mathbf{F}(\mathbf{r}) - k_B T \nabla \rho(\mathbf{r}) = 0, \quad (2)$$

where the total (deterministic) one-body force density distribution is given by

$$\mathbf{F}(\mathbf{r}) = \left\langle \sum_i \mathbf{f}_i(\mathbf{r}^N) \delta(\mathbf{r} - \mathbf{r}_i) \right\rangle, \quad (3)$$

with the total force acting on particle i being

$$\mathbf{f}_i(\mathbf{r}^N) = -\nabla_i u(\mathbf{r}^N) - \nabla_i V_{\text{ext}}(\mathbf{r}_i), \quad (4)$$

where ∇_i is the derivative with respect to \mathbf{r}_i , $u(\mathbf{r}^N)$ is the interparticle interaction potential ($\mathbf{r}^N = \mathbf{r}_1 \dots \mathbf{r}_N$), and $V_{\text{ext}}(\mathbf{r})$ is the external potential. In Eq. (2), k_B is the Boltzmann constant, and T is temperature.

In short, having sampled $\mathbf{F}(\mathbf{r})$ allows us to integrate (2) in space in order to obtain results for $\rho(\mathbf{r})$. In particular, for effectively one-dimensional problems, carrying out a simple one-dimensional integration (along z) is all that is required. In the general case, a line integral needs to be performed,

$$\rho(\mathbf{r}) = \rho_0 + (k_B T)^{-1} \int_{\Gamma} ds \cdot \mathbf{F}(\mathbf{r}), \quad (5)$$

where Γ represents an appropriate path that connects (say) the origin with position \mathbf{r} , and ds is the differential line element. The integral in Eq. (5) determines the density profile up to an additive constant, ρ_0 , that can be determined by imposing the correct normalization.

Alternatively, we can invert Eq. (2)

$$\rho(\mathbf{r}) = \rho_0 + (k_B T)^{-1} \nabla^{-1} \cdot \mathbf{F}(\mathbf{r}), \quad (6)$$

applying the inverse operator ∇^{-1} to the force density field

$$\nabla^{-1} \cdot \mathbf{F}(\mathbf{r}) = \frac{1}{c_d} \int d\mathbf{r}' \frac{\mathbf{r} - \mathbf{r}'}{|\mathbf{r} - \mathbf{r}'|^d} \cdot \mathbf{F}(\mathbf{r}'), \quad (7)$$

where d indicates the dimensionality of the system and the constant $c_d = 4\pi$ if $d = 3$ and $c_d = 2\pi$ if $d = 2$ [25].

The advantage of the force sampling method is that it only samples the (non-trivial) interaction contribution (3). The (ideal gas) diffusive term, $-k_B T \nabla \rho$, is treated explicitly. This is in contrast to sampling $\rho(\mathbf{r})$ directly via Eq. (1), where these trivial fluctuations induce a very significant fluctuating background which besets the data.

To illustrate the accuracy of the new method we carry out Monte Carlo (MC), Brownian Dynamics (BD), and Molecular Dynamics (MD) simulations. We compare the density profiles obtained via the traditional counting method and the force balance sampling.

In order to have the possibility to provide quasi-exact data, against which to gauge both methods, we study a system with $N = 25$ particles interacting via the Lennard-Jones (LJ) 6-12 potential. Hence, the interparticle potential between two particles separated by a distance r is $\phi(r) = 4\epsilon \left[\left(\frac{\sigma}{r}\right)^{12} - \left(\frac{\sigma}{r}\right)^6 \right]$. We set $\epsilon = 1$ and $\sigma = 1$ as the units of energy and length, respectively. The particles are located in a square box of side length $L = 10\sigma$ with periodic boundary conditions. The particles are in equilibrium in an external potential $V_{\text{ext}}(x) = V_0 \sin(2\pi n_w x/L)$, that depends only on the x -coordinate. We fix $V_0/\epsilon = 0.01$ and $n_w = 5$. The

temperature is $k_B T/\epsilon = 1$. We impose a relatively small external potential, such that the resulting equilibrium $\rho(x)$ is rather flat. The profile shows peak-to-peak oscillations of $\sim 1\%$ relative to the average density. Sampling such small differences in the density profile is highly demanding and therefore constitutes a strong test for the force sampling method. A schematic of the system and plots of both ρ and V_{ext} are shown in the Supplemental material [26].

In Fig. 1a we compare density profiles obtained via counting and force sampling in MC simulations with a number of Monte Carlo steps (MCS) ranging from 10^7 to 10^{11} . In a MCS each particle is once attempted to be moved. The statistical noise is significantly smaller in the density profiles obtained via force sampling. Even after 10^{11} MCS density fluctuations are still far from negligible when using the traditional counting method. We have obtained similar differences between both methods in BD and MD.

To quantify the accuracy of both methods, we define the sampling error Δ of the density profile as

$$\Delta = \frac{\int d\mathbf{r} |\rho_s(\mathbf{r}) - \rho_{\text{eq}}(\mathbf{r})|}{\int d\mathbf{r} \rho_{\text{eq}}(\mathbf{r})}. \quad (8)$$

Here ρ_s is the sampled density profile and ρ_{eq} represents the "true" equilibrium profile. An accurate estimation of ρ_{eq} is obtained by running a very long MC simulation (10^{12} MCS) and defining ρ_{eq} as the average profile obtained with both methods, counting and force sampling.

Fig. 1b shows the sampling error in MC, BD, and MD simulations. In all cases force sampling performs significantly better than the traditional counting method. To achieve a given sampling error Δ with traditional counting we need simulations ~ 6 times longer than using force sampling. In other words, force sampling reduces the computation time by $\sim 80\%$.

The traditional counting method ensures by construction the correct normalization of $\rho(\mathbf{r})$. This is not true when using force sampling. Here, an additive constant must be added to normalize the density profile. This constant together with the accumulation of the error in the spatial integral, cf. (5) might introduce small artifacts such as slightly asymmetric density profiles in symmetric systems or negative values of the density. To illustrate this effect we introduce a parabolic external potential $V_{\text{ext}}(x) = V_0(x - L/2)^2$, with $V_0/\epsilon = 5$. Given the strength of the potential, the particles strongly accumulate in a small region around $x = L/2$ and the density vanishes in the rest of the simulation box. Due to the normalization of ρ , force sampling erroneously yields a non-zero density value far from $x = L/2$ (positive for $x \ll L/2$ and negative for $x \gg L/2$), see Fig. 2a. This anomalous behaviour introduces a relevant error only if the sampling is clearly insufficient. Nevertheless, one must be aware that even a small error might be relevant to the calculation of e.g. free energies. One can partially alleviate this

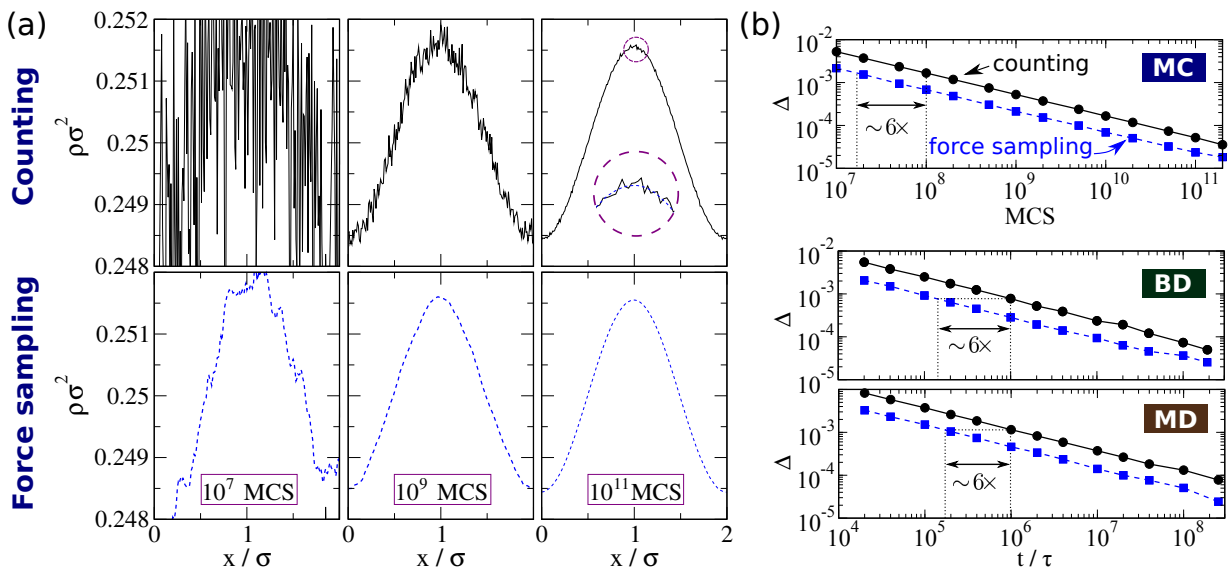


FIG. 1. (a) Density profiles obtained with MC simulations for different numbers of MCS, as indicated. The bin size is $\Delta x/\sigma = 0.01$, $N = 25$, and $L/\sigma = 10$. The top panels show $\rho(x)$ obtained via the traditional counting method (black-solid lines). The density profiles obtained via force sampling are represented in the bottom panels (blue-dashed lines). The inset in the top panel with 10^{11} MCS is a close view of both methods in the vicinity of the density peak. Only one fifth of the simulation box, $x/\sigma \in [0, 2]$, corresponding to one density peak is represented. (b) Logarithmic plots of the sampling error Δ as a function of: (i) the number of Monte Carlo steps in MC simulations (top), (ii) the simulation time t/τ in BD simulations (middle) and MD simulations (bottom). In BD the time is measure in units of $\tau = \sigma^2\gamma/\epsilon$ with $\gamma = 1$ the friction coefficient. In MD, $\tau = \sigma\sqrt{m/\epsilon}$ with $m = 1$ the mass of the particles. Data obtained via counting (black circles) and via force sampling (blue squares).

anomaly imposing zero density in the regions where no particles have been detected during the simulation.

If the density varies significantly from minimum to maximum, then the profiles obtained with both methods might at first look almost identical. However, building the numerical derivatives of $\rho(\mathbf{r})$ with respect to the spatial coordinates reveals the higher accuracy of force sampling, see Fig. 2b.

Another example with local high density values is shown in the Supplemental Material [26]. Force sampling is more accurate and generate smoother profiles than the counting method also at high densities. The reduction in the sampling error is, however, less pronounced than in the case of smooth density profiles. We find that force sampling reduces the computation time by $\sim 40\%$.

The small system size $N = 25$ investigated so far has enabled us to carry out a detailed statistical analysis of the relative performance of the two methods. Nevertheless, the force sampling method remains useful in systems with more realistic values of N .

In the Supplemental Material [26] we show a comparison of the density profiles obtained with MC via counting and force sampling in a system with $N = 10^3$ and the same "soft" external potential as in Fig. 1. Force sampling is ~ 5 times more accurate than counting.

We discuss next the effect of varying the size of the bin. The results shown previously were obtained at a

fixed bin size $\Delta x/\sigma = 0.01$. Reducing the size of the bin increases the level of detail with which we can sample the density profile. On the other hand, in the traditional counting method the error in the density profile also increases by reducing the size of the bin since the number of events contributing to each bin is proportional to the volume of the bin. In contrast, the error in the force sampling method does not significantly depend on the size of the bin. The reason is that, in contrast to the counting method, the density at each bin is not determined by the local number of events but via a spatial integral of the force density. Fig. 3 shows the sampling error as a function of the bin size. The data was obtained using MC simulations with 10^9 MCS. The external potential, number of particles, and temperature are the same as those in Fig. 1.

Systems that require a small bin size, such as for example cases where the density profile depends on two or three spatial coordinates, will substantially benefit from applying the force sampling method. To illustrate this we introduce the external potential $V_{\text{ext}}(\mathbf{r}) = V_0 \sin(2\pi n_w x/L) \sin(2\pi n_w y/L)$, that depends on both x - and y -coordinates. We fix $V_0/\epsilon = 1$ and $n_w = 5$. The resulting two-dimensional (2D) density profile is shown in Fig. 4. Force sampling is clearly superior to counting. Details on how to obtain the 2D density profile using force sampling are given in the Supplemental Mate-

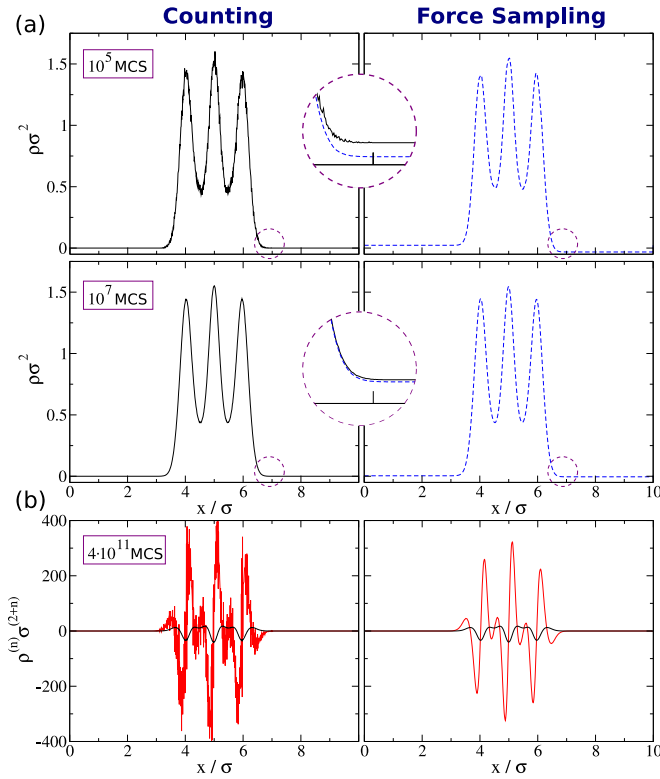


FIG. 2. (a) Density profiles obtained with MC simulations using counting (left) and force sampling (right). The number of MCS is 10^5 (top panels) and 10^7 (bottom panels), as indicated. The bin size is $\Delta x/\sigma = 0.01$. The particles are in equilibrium in an external parabolic potential. The insets are close views of the region where the density vanishes. Using force sampling the density in this region reaches an artificial negative value of $\sim -2 \cdot 10^{-2}$ for 10^5 MCS and $\sim -4 \cdot 10^{-3}$ for 10^7 MCS. (b) Second $\rho^{(2)}$ (black lines) and third $\rho^{(3)}$ (red lines) numerical derivatives (centered difference) of $\rho(x)$ with respect to x , $\rho^{(n)}(x) = \partial^n \rho(x)/\partial x^n$. Data obtained via counting (left) and force sampling (right) in a MC simulation with $4 \cdot 10^{11}$ MCS.

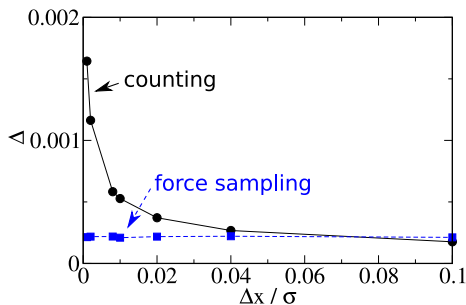


FIG. 3. Sampling error Δ as a function of the bin size. Data obtained via counting (black circles) and force sampling (blue squares), using MC simulations with 10^9 MCS. The "true" equilibrium profile used to compute Δ is approximated by the average profile of both methods after 10^{12} MCS.

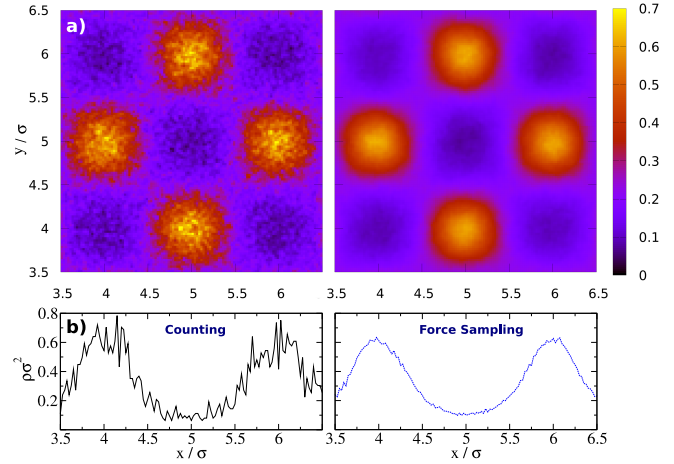


FIG. 4. (a) Contour plots of the equilibrium 2D density profile in the external potential $V_{\text{ext}}(\mathbf{r}) = V_0 \sin(2\pi n_w x/L) \sin(2\pi n_w y/L)$ with $V_0/\epsilon = 1$ and $n_w = 5$. Data obtained with 10^6 MCS using counting (left) and force sampling (right). The bins are squares of side length 0.025σ . The simulation box is a square of side length 10σ . Only the central region of the box is shown. (b) Density profile vs. x at constant $y/\sigma = 5$ obtained via counting (left) and force sampling (right).

rial [26].

Implementing the force sampling method is straightforward in all simulation techniques analyzed here and its computational demand is negligible in both BD and MD, and very low in MC. Note that in MC we need to implement the calculation of the forces (not inherent in the method) and compute them every certain number of MCS as part of the sampling process. We sample the force density during the whole simulation, but it is only at the end of the simulation run that we compute $\rho(\mathbf{r})$ via spatial integration of the force density, cf. (5).

The force sampling method cannot be directly used in hard core systems (i.e., particles interact only if they overlap, in which case the interparticle potential is infinity). However, a hard core system can be approximated by a quasihard potential that decays very fast with the distance between the particles.

It might also be possible to extend the force sampling method to study hard core systems using Event Driven Molecular [27] and Brownian [28, 29] Dynamics since in both cases the moment transfer in a collision is available.

Besides the examples shown here, we have tested the validity and accuracy of force sampling in a one-dimensional system of quasihard spheres ($\phi(r) \propto r^{-42}$) and in one- and two-dimensional systems of Gaussian particles. In all cases the force sampling method has provided better accuracy than the standard counting method.

Finally we have also verified the better performance of the method in a 2D system of Gaussian particles un-

der stationary shear conditions [30]. In steady state the method is still valid for those Cartesian components for which Eq. (2) still holds, such as e.g. in the direction perpendicular to the shear flow. Furthermore, in BD it is also possible to apply the force sampling method to out-of-equilibrium conditions, even away from steady-states. In out-of-equilibrium BD the force density balance at any time t is given by

$$\mathbf{F}(\mathbf{r}, t) - k_B T \nabla \rho(\mathbf{r}, t) = \mathbf{J}(\mathbf{r}, t), \quad (9)$$

where \mathbf{J} is the one-body current, which in contrast to the equilibrium case, Eq. (2), does not vanish in general. Therefore in addition to the sampling of the forces it is also necessary to sample the total current to be able to obtain the density profile via spatial integration. Sampling the current, which is possible using the numerical derivative of the position vector or via the continuity equation, might increase the statistical noise with respect to the equilibrium case. Therefore, it is not guaranteed that force sampling will perform better than counting in out-of-equilibrium. This study constitutes the subject of future work. Adding inertial terms to Eq. (9) would allow the extension of the method to out-of-equilibrium MD.

The generalization of the method to multicomponent mixtures is straightforward. Testing the performance in grand canonical MC schemes [3] is an interesting research task for the future.

We thank N. B. Wilding, E. Chacón, M. Dijkstra, M.P. Allen, and D. Borgis for feedback and stimulating discussions, and D. Borgis for pointing out Ref. [21] to us.

SUPPLEMENTAL MATERIAL: BETTER THAN COUNTING: DENSITY PROFILES FROM FORCE SAMPLING

System

A schematic of the system is shown in Supplemental Fig. 5a. The external potential and the corresponding equilibrium density profile are shown in Supplemental Fig. 5b and c, respectively.

High density states

An example exhibiting local high density values is shown in Supplemental Fig. 6. The particles are in equilibrium in the same type of external potential as that shown in Fig. 1b of the main text, that is $V_{\text{ext}}(x) = V_0 \sin(2\pi n_w x/L)$ with $n_w = 5$, but much stronger, $V_0/\epsilon = 3$. As a result the density profile shows strong oscillations, see Supplemental Fig. 6a. The force sampling method is more accurate and generates smoother profiles than the counting method. The reduction in the sampling error is, however, less pronounced than in cases

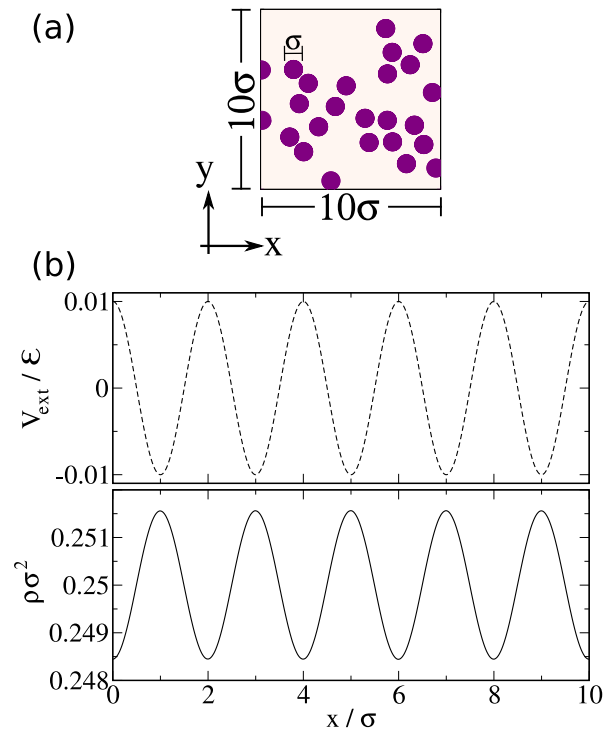


FIG. 5. (a) Schematic of the system, $N = 25$ LJ particles of size σ in a square box of side length 10σ with periodic boundary conditions. (b) External potential (top) and corresponding equilibrium density profile (bottom) obtained with MC simulation (10^{12} Monte Carlo steps).

with smooth density profiles. To achieve a given sampling error Δ with traditional counting we need simulations ~ 2 times longer than using force sampling, see Supplemental Fig. 6b. That is, force sampling reduces the computation time by $\sim 40\%$.

Realistic number of particles

In Supplemental Fig. 7a we show a comparison of the density profiles obtained with MC via counting and force sampling a system with $N = 10^3$. The particles are in a rectangular box with side lengths $L_x/\sigma = 10$ and $L_y/\sigma = 400$ subject to the external potential shown in Fig. 5b. Therefore, the system is homogeneous in the y -coordinate. In Supplemental Fig. 7b we show the sampling error Δ of both methods in MC. Force sampling is ~ 5 times more accurate than counting. The "true" equilibrium profile used to compute the sampling error Δ is approximated here by the average profile given by both methods after $2 \cdot 10^{10}$ MCS (obtained by averaging $2 \cdot 10^3$ MC simulations of 10^7 MCS each).

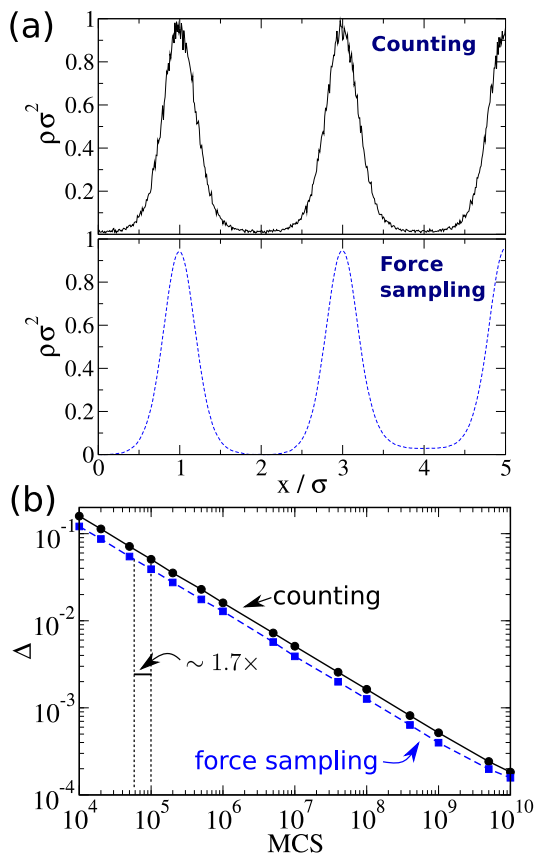


FIG. 6. (a) Density profiles obtained with MC simulations using the counting (top) and the force sampling (bottom) method. The number of MCS is 10^4 and the bin size is $\Delta x/\sigma = 0.01$. The size of the box is $L/\sigma = 10$ (only half of the box is shown) and $N = 25$. The particles are in equilibrium in the external potential $V_{\text{ext}}(x) = V_0 \sin(2\pi n_w x/L)$ with $n_w = 5$ and $V_0/\epsilon = 3$. The temperature is $k_B T/\epsilon = 1$. (b) Logarithmic plot of the sampling error Δ as a function of the number of Monte Carlo steps. Data obtained via counting (black circles) and via force sampling (blue squares). The "true" equilibrium profile used to compute Δ is approximated by the average profile given by both methods after $4 \cdot 10^{11}$ MCS.

Multidimensional density profiles

If the density profile depends on several spatial coordinates, there are at least three routes to implement the force sampling method. One possibility, as described in Eq. (5) of the main text, is to perform a line integral of the force density. Alternatively, we can invert the force density balance equation and obtain the density profile via a volume integral over the full space, see Eqs. (6) and (7) of the main text. Eq. (7) of the main text can be solved either in real or in Fourier space (see Ref. [21] of the main text) a post processing of the data sampled during the simulation. Finally, we can also obtain the density profile via numerical minimization of the func-

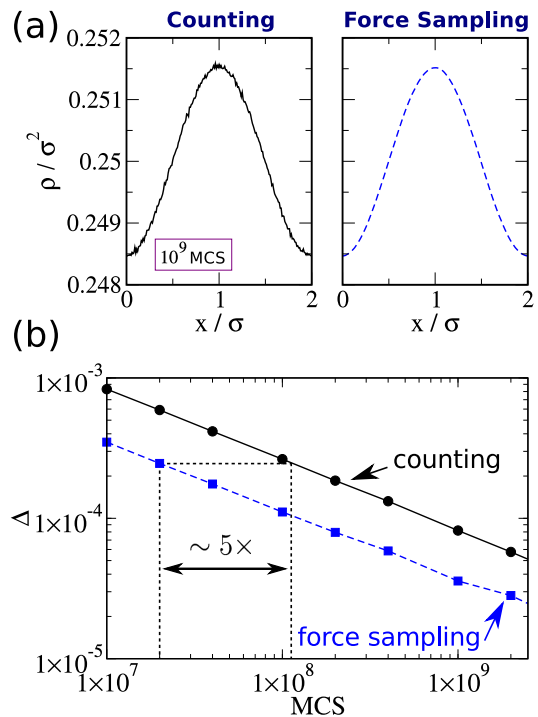


FIG. 7. (a) Density profiles (MC simulation with 10^9 MCS) obtained via counting (left) and force sampling (right) in a system with $N = 10^3$ confined in a box with side lengths $L_x/\sigma = 10$ and $L_y/\sigma = 400$. The bin size is $\Delta x/\sigma = 0.01$. The particles are in equilibrium in the external potential $V_{\text{ext}}(x) = V_0 \sin(2\pi n_w x/L_x)$, with $V_0/\epsilon = 0.01$ and $n_w = 5$. Only one fifth of the simulation box is shown, $x/\sigma \in [0, 2]$. (b) Logarithmic plot of the sampling error as a function of the number of MCS.

tional

$$H[\rho] = \int d\mathbf{r} \|\nabla \rho(\mathbf{r}) - \mathbf{F}(\mathbf{r})\|^2, \quad (10)$$

which is a standard procedure to numerically find the scalar potential that generates a given curl-free vector field. In practice, inverting the force balance equation via Eq. (7) of the main text, or numerically minimizing $H[\rho]$ results in more accurate density profile than solving the line integral in Eq. (5) of the main text. Note that both inversion of the force balance equation and minimization of $H[\rho]$ use information from the whole system in order to compute the local density profile at position \mathbf{r} . The two-dimensional density profiles shown in Fig. 4 (right) of the main text have been obtained via minimization of $H[\rho]$.

-
- [1] J. H. Sikkenk, J. O. Indekeu, J. M. J. van Leeuwen, and E. O. Vossnack, Phys. Rev. Lett. **59**, 98 (1987).
 [2] J. E. Finn and P. A. Monson, Phys. Rev. A **39**, 6402 (1989).

- [3] A. Macioek, R. Evans, and N. B. Wilding, *J. Chem. Phys.* **119**, 8663 (2003).
- [4] S. Auer and D. Frenkel, *Phys. Rev. Lett.* **91**, 015703 (2003).
- [5] E. Chacón and P. Tarazona, *Phys. Rev. Lett.* **91**, 166103 (2003).
- [6] A. Parmeggiani, T. Franosch, and E. Frey, *Phys. Rev. Lett.* **90**, 086601 (2003).
- [7] D. T. Limmer, C. Merlet, M. Salanne, D. Chandler, P. A. Madden, R. van Roij, and B. Rotenberg, *Phys. Rev. Lett.* **111**, 106102 (2013).
- [8] A. Härtel, *J. Phys.: Condens. Matter* **29**, 423002 (2017).
- [9] A. Fortini, D. de las Heras, J. M. Brader, and M. Schmidt, *Phys. Rev. Lett.* **113**, 167801 (2014).
- [10] T. Biben, R. Ohnesorge, and H. Löwen, *EPL* **28**, 665 (1994).
- [11] A. Torres, A. Cuetos, M. Dijkstra, and R. van Roij, *Phys. Rev. E* **75**, 041405 (2007).
- [12] D. de las Heras, L. L. Treffenstädt, and M. Schmidt, *Phys. Rev. E* **93**, 030601 (2016).
- [13] N. D. Mermin, *Phys. Rev.* **137**, A1441 (1965).
- [14] R. Evans, *Adv. Phys.* **28**, 143 (1979).
- [15] R. Davidchack, B. Laird, and R. Roth, *Condens. Matter Phys.* **19**, 23001 (2016).
- [16] C. P. Royall, J. Dzubiella, M. Schmidt, and A. van Blaaderen, *Phys. Rev. Lett.* **98**, 188304 (2007).
- [17] D. G. A. L. Aarts, M. Schmidt, and H. N. W. Lekkerkerker, *Science* **304**, 847 (2004).
- [18] G. Volpe, T. Brettschneider, L. Helden, and C. Bechinger, *Opt. Express* **17**, 23975 (2009).
- [19] R. Piazza, S. Buzzaccaro, E. Secchi, and A. Parola, *Soft Matter* **8**, 7112 (2012).
- [20] D. Martin-Jimenez, E. Chacon, P. Tarazona, and R. Garcia, *Nat. Commun.* **7**, 12164 (2016).
- [21] D. Borgis, R. Assaraf, B. Rotenberg, and R. Vuilleumier, *Mol. Phys.* **111**, 3486 (2013).
- [22] R. Assaraf, M. Caffarel, and A. Scemama, *Phys. Rev. E* **75**, 035701 (2007).
- [23] S. Fritsch, S. Pobleto, C. Junghans, G. Ciccotti, L. Delle Site, and K. Kremer, *Phys. Rev. Lett.* **108**, 170602 (2012).
- [24] J.-P. Hansen and I. R. McDonald, *Theory of simple liquids*, 4th ed. (Academic Press, Amsterdam, 2013).
- [25] Note that in Ref. [21] the authors suggest in words the present method below their Eq.(22), using Fourier space to solve the quadrature (5).
- [26] See supplemental material for details.
- [27] B. J. Alder and T. E. Wainwright, *J. Chem. Phys.* **27**, 1208 (1957).
- [28] P. Strating, *Phys. Rev. E* **59**, 2175 (1999).
- [29] A. Scala, T. Voigtmann, and C. D. Michele, *J. Chem. Phys.* **126**, 134109 (2007).
- [30] N. C. X. Stuhlmüller, T. Eckert, D. de las Heras, and M. Schmidt, Submitted (2018).